Available online at www.sciencedirect.com
SCIENCE DIRECT®
Journal of Power Sources 136 (2004) 154–159
JOURNAL OF POWER SOURCES
www.elsevier.com/locate/jpowsour

Short communication

# Microstructure and electrochemical properties of a nanometer-scale tin anode for lithium secondary batteries

Wanuk Choi [a,b], Jeong Yong Lee [a,*], Bok Hwan Jung [b], Hong Sup Lim [b]

[a] *Department of Materials Science and Engineering, Korea Advanced Institute of Science and Technology, Daejeon 305-701, Republic of Korea*
[b] *Energy Lab, Samsung SDI Corporate R&D Center, Yongin-si, Gyeonggi-do 449-575, Republic of Korea*

Received 2 February 2004; accepted 17 May 2004

Available online 30 July 2004

**Abstract**

The microstructure of nanometer-scale tin powder synthesized by the wire electric explosion (WEE) method is examined by transmission electron microscopy (TEM) at different Li insertion states, and then electrochemical properties of the tin power electrode are characterized by galvanostatic charge–discharge experiments. It is found that several Li/Sn inter-metalic compounds are formed during lithium insertion, namely $Li_{1-x}Sn$, $L_{13}Sn_5$ and $Li_7Sn_2$. The passivation layer (or solid electrolyte interface, SEI) on the surface of particles cycled in an organic electrolyte electrochemical cell is characterized as $Li_2CO_3$ and $ROCO_2Li$ by FT-IR spectroscopy. A great part of the passivation layer is amorphous, but a small is poorly crystallized.


*Keywords:* Nanometer-scale; Tin anode; Passivation layer; Lithium secondary battery

## 1. Introduction

Recently, lithium-ion secondary batteries have been widely used as energy-storage devices for portable electronic goods, such as cellular phones, notebook computers and camcorders. As anode materials for lithium-ion cells, various carbonaceous materials have been considered. For example artificial graphite, hard carbon and natural graphite have been widely commercialized [1,2].

In addition to carbonaceous materials, attention has also been focused on alloys because of their high specific gravitational and volumetric capacities (e.g., Li/Sn: 994 mAh $g^{-1}$, Li/Sb: 660 mAh $g^{-1}$, Li/graphite: 372 mAh $g^{-1}$) [3–5]. An early study by Dey [6] showed that Li formed alloys with various metals in an organic electrolyte electrochemical cell [6]. Many research groups have investigated the compositional change and thermodynamic properties of lithium alloys in lithium salt cells at high temperatures and in an organic electrochemical cells at ambient temperatures [7–12]. Huggins [12] found by means of coulometric titration that tin-based material form various inter-metallic compounds, such as LiSn, $Li_5Sn_2$, $Li_{13}Sn_5$, $Li_7Sn_2$ and $Li_{22}Sn_5$, both at high temperatures and at ambient temperature. Courtney and Dahn [13] reported similar results from in situ X-ray diffraction (XRD) [13]. Regardless of high gravitational and volumetric capacity, none of metallic and alloy systems have been commercialized. The difficulty of using alloy systems as anodes for lithium ion batteries is due to the poor integrity of the electrode on charge–discharge cycling. The volume changes during insertion and de-insertion of lithium result in a large mechanical strain, which brings about pulverization of the electrode. In several studies, substances that contain reduced particle size and multi-phases have enhanced the cycle characteristics of alloys as anodes [14,15].

In this study, nanometer-scale tin powder has been prepared by the wire electric explosion (WEE) method. This method is a type of pulse energy technology that is suitable for ultra-fine powder production. The products can be controlled precisely and the WEE method proceeds is extremely fast compared with alternative procedures. These transmission electron microscopy (TEM) has been used to investigate Li/Sn alloys during the electrochemical Li insertion process in an organic electrolyte electrochemical cell and the electrochemical properties of a nanometer-scale tin electrode has been characterized by charge–discharge experiments. The components of the passivation layer on the surface of the tin particles cycled in the organic electrolyte electrochemical cell have been analyzed by FT-IR spectroscopy and the microstructure and thickness have been observed by high-resolution transmission electron microscropy (HRTEM).

* Corresponding author. Tel.: +82 42 869 4216; fax: +82 42 869 4276.
*E-mail address:* j.y.lee@kaist.ac.kr (J.Y. Lee).

0378-7753/$ – see front matter © 2004 Elsevier B.V. All rights reserved.
doi:10.1016/j.jpowsour.2004.05.026

## 2. Experimental

The nanometer-scale tin powders were synthesized by the WEE method. First, tin powder (Aldrich Chemical Co., 99.9%) was melted in an argon atmosphere and then extruded to a wire of 0.2 mm diameter. The extruded wire was exploded within an adiabatic chamber filled with argon by supplying an electric pulse [16]. The structure and morphology of the exploded tin powder were characterized by means of X-ray diffraction (Rigaku Co., Geigeflex), BET specific-surface area (Micromeritics Co., ASAP-2000) and scanning electron microscopy (SEM) (Phillips Co., XL30). For TEM observations, the electrodes were prepared by coating a slurry of active material powder (90 wt.%) and carbon black (10 wt.%) dispersed in *n*-methyl pyrrolidine on to a Ni form. The electrodes for measurement of electrochemical characteristics were prepared by coating a slurry of active material powder (80 wt.%), carbon black (10 wt.%) and polyvinylidine fluoride (10 wt.%) dissolved in *n*-methyl pyrrolidine on to a Cu foil substrate.

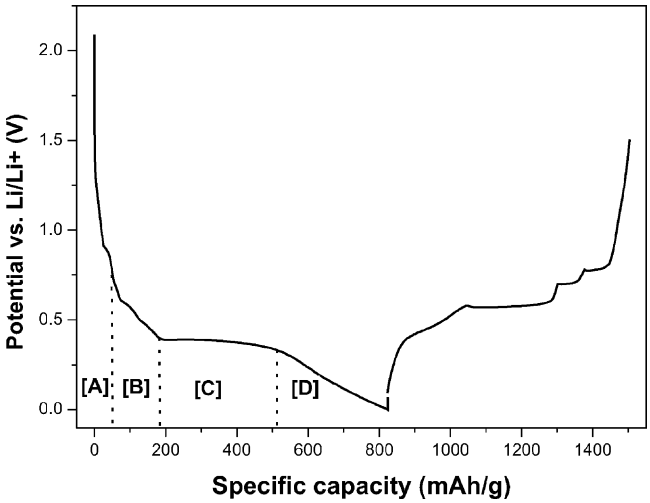


Fig. 2. Voltage vs. capacity of nanometer-scale Sn/Li cell in 1.3 M $L1PF_6$/EC-DMC (3:7) cycled at constant current density, 0.2 mA $cm^{-2}$.

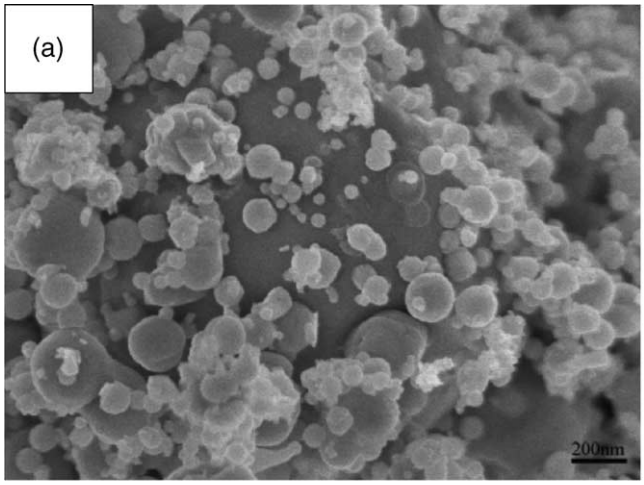


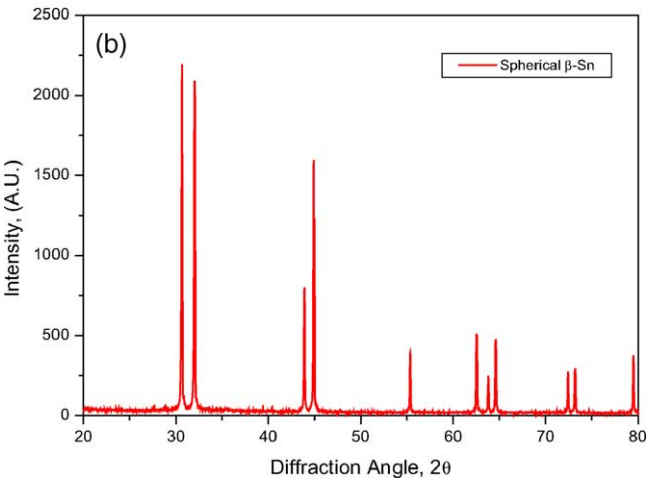


Fig. 1. SEM photograph and X-ray diffraction pattern of Sn powder prepared by WEE method.

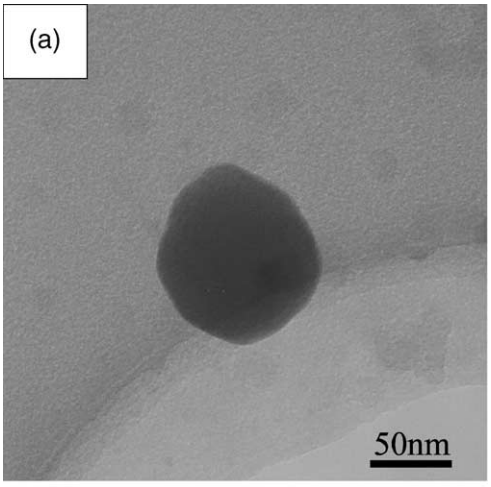


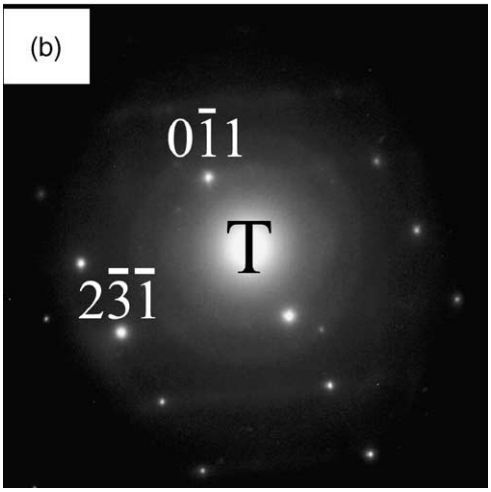


Fig. 3. TEM bright-field image and diffraction pattern of Sn powder discharged to 0.7 V (region A in Fig. 2).

FT-IR measurements were performed with electrodes prepared by coating a slurry of active material powder (90 wt.%) and polyvinylidine fluoride (10 wt.%) dissolved in *n*-methyl pyrrolidine on to a Cu foil substrate. The electrodes were assembled in 2016 type coin cells in an argon-filled glove box (Vac Co.) using Celgard 2400 as a separator, 1.3 M $LiPF_6$ in a 3:7 mixture of ethylene carbonate/diethyl carbonate as an electrolyte, and lithium foil as a counter electrode. The charge–discharge experiments were performed galvanostatically between 0.01 and 1.5 V at 0.2 mA $cm^{-2}$. The TEM studies of tin powders charged with lithium in different states were carried out with a JEM2000EX instrument (Jeol Co.). The samples were prepared in glove box and transferred to the microscope and FT-IR analyzer (Nicolet, NEXUS870).

## 3. Results and discussion

A SEM image that reveals the morphology of the tin powders synthesized by WEE method is given in Fig. 1(a). The size of the small particles is about a few tens of nm and that of large particles is about 200 nm. The particle shape of the synthesized tin powder is spherical and the surface of is very smooth. The BET surface area of is 4.847 $m^2\ g^{-1}$, which is not as large as that of nanometer-scale $SnO_2$. X-ray diffraction data indicates that the phase of the synthesized powders is β-Sn (Fig. 1(b)). Very small peaks of SnO and $SnO_2$ are also observed at around 27–28°, which means that a small amount of the β-Sn particles is partially oxidized.

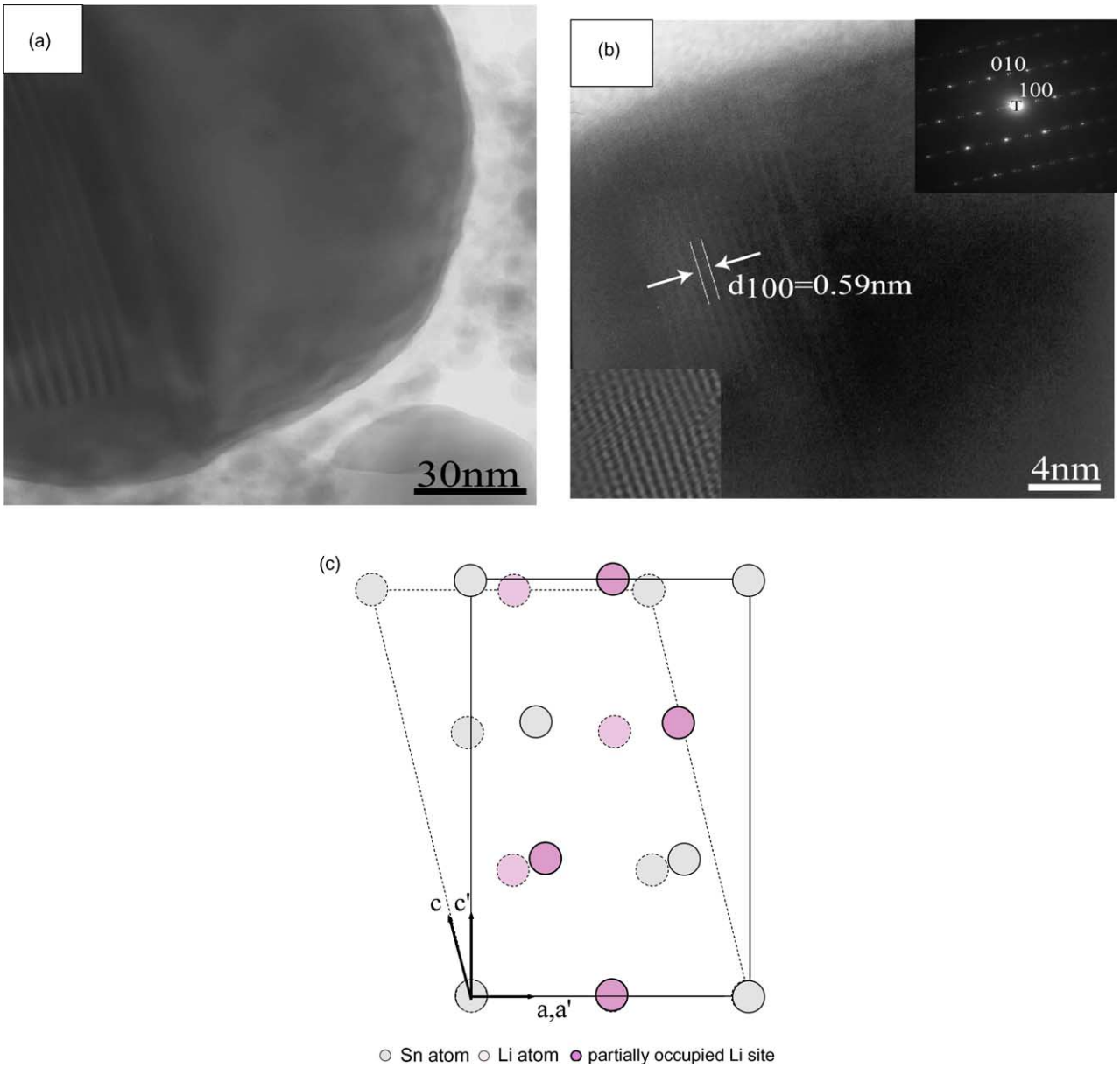


Fig. 4. TEM bright-field image and high-resolution TEM image of Sn powder discharged to 0.5 V (region B in Fig. 2) and structure of LiSn (dotted line) and $Li_{1-x}Sn$ (solid line) viewed through *c* axis.

A charge–discharge curve for the nanometer-scale tin powder is shown in Fig. 2. The first discharge (Li insertion) curve of synthesized tin powder has four plateaux: the first at 0.8 V, the second at 0.6 V, the third at around 0.53 V and the fourth at 0.4 V. By contrast, the first charge (Li de-insertion) curve exhibits three plateau: one at 0.69 V and the others at 0.81 and 0.91 V. The shoulder of discharge curve at 1.5 V is associated with electrolyte decomposition [17]. The plateau of the discharge curve at around 0.8 V disappears in the charge curve. Therefore, the reaction at 0.8 V during discharge is irreversible and is the decomposition of tin oxide the surface of the synthesized tin powder. The following plateaux are the formation of lithium–tin alloy phases. Courtney and Dahn [13] reported that various tin oxide based compounds, such as SnO, $SnO_2$ and $SnSiO_3$, were formed to lithium oxide and lithium metal first by introducing Li into tin-based materials and then followed the formation of the various Li–Sn alloy compounds [13].

Samples from the different Li insertion states, A, B, C and D in Fig. 2 were obtained for TEM analysis, The lithiated Sn particles from the A region have a β-Sn phase. Fig. 3(a) and (b) show the bright-field image and the [2 1 1] diffraction pattern of the β-Sn phase, respectively. An oxide layer was not observed on the synthesized tin powder. This suggest that in tin oxide decomposition had taken place. The bright-field image and HRTEM image of $Li_{1-x}Sn$ particles obtained from B region in Fig. 2 are presented in Fig. 4. The zone direction of the diffraction pattern of $Li_{1-x}Sn$ is [0 0 1] and the (1 0 0) lattice can be seen in the HRTEM image. The bottom left-side of the HRTEM image is a processed image of the $Li_{1-x}Sn$ (1 0 0) planes, which is clearer than the original lattice image. The processed image was obtained from the real HRTEM image by Fourier transformation, noise reduction and reverse-Fourier transformation. The chemical formula of the particles obtained from B region in Fig. 2 can be written as $Li_{1-x}Sn$ instead of LiSn, because the diffraction pattern of $Li_{1-x}Sn$ (Fig. 4(b)) is different from that of LiSn and the inserted Li content in region B is less than that for LiSn formation. Huggins [12] calculated the equilibrium potential of the plateaux in the Li–Sn–O ternary system at ambient temperature and reported that lithium–tin alloys, such as $Li_{0.4}Sn$ and $Li_{0.714}Sn$, were formed during electrochemical reaction with Li [11]. LiSn has a monoclinic structure, i.e., $a = 5.17$ Å, $b = 3.18$ Å, $c = 7.74$ Å, $\beta = 104.5^\circ$, and its space group is $P2/m$ [18]. By contrast, the [0 0 1] diffraction pattern of $Li_{1-x}Sn$ is well-defined as orthorhombic, i.e., $a = 5.17$ Å, $b = 3.18$ Å, $c = 7.74$ Å. A schematic drawing of the Li and Sn atoms in the (0 1 0) planes of the LiSn structure is given in Fig. 4(c). The LiSn monoclinic structure (dotted line in Fig. 4(c)) has two types of Li site, one is the centre of a Sn prism and the other is the centre of a Sn quadrangle. The former is more a open interstitial site and therefore Li ion insertion is such a site is dominant. The shear stress induced by transforming from a tetragonal Sn to a Li-deficient structure phase, $Li_{1-x}Sn$, should be less than that induced by transformation from Sn to LiSn. Therefore, distrotion of the $Li_{1-x}Sn$ structure versus that of the Sn structure (tetragonal, $a = 5.83$ Å, $c = 3.18$ Å) is less than that of LiSn. It is proposed that the $Li_{1-x}Sn$ structure is formed prior to LiSn during Li insertion into tin metal powder and that the LiSn structure should be followed by further uptake of Li. The reaction at around 0.5 V during Li insertion can be represented by:

$$(1 - x)\mathrm{Li} + \mathrm{Sn} = \mathrm{Li}_{1-x}\mathrm{Sn} \quad (x < 1) \tag{1}$$

$$x\mathrm{Li} + \mathrm{Li}_{1-x}\mathrm{Sn} = \mathrm{LiSn} \tag{2}$$

A $Li_{13}Sn_5$ structure is observed by TEM within particles discharged to below 0.5 V. Fig. 5(a) is a bright-field image

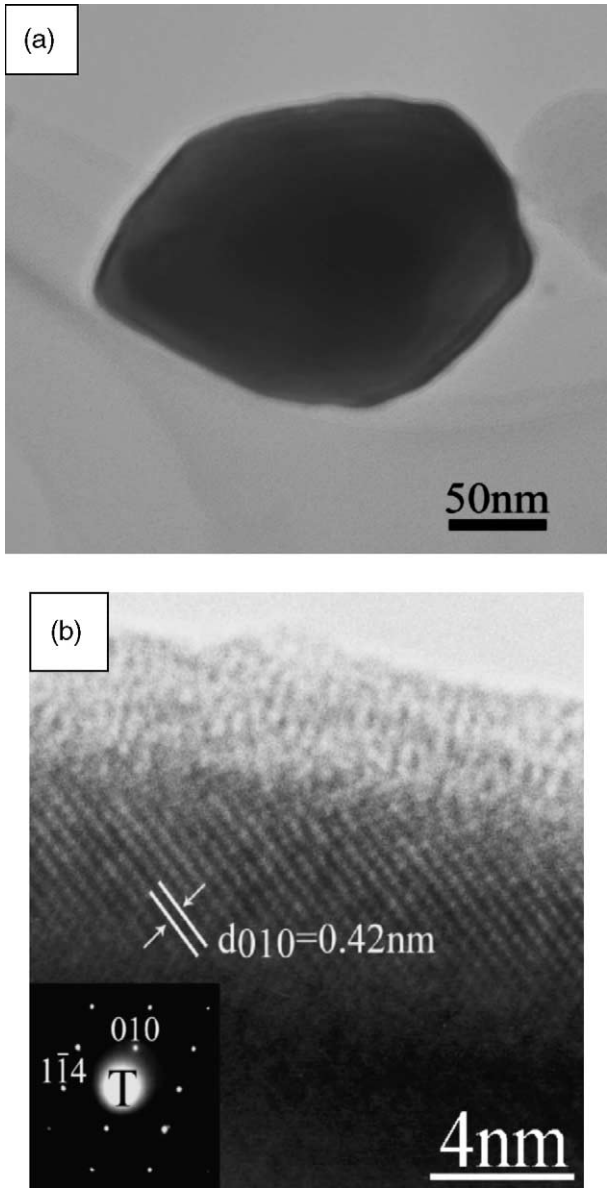


Fig. 5. Bright-field and high-resolution TEM image of lithiated Sn particle ($Li_{13}Sn_5$) discharged to below 0.5 V at constant current density, 0.2 mA $cm^{-2}$.

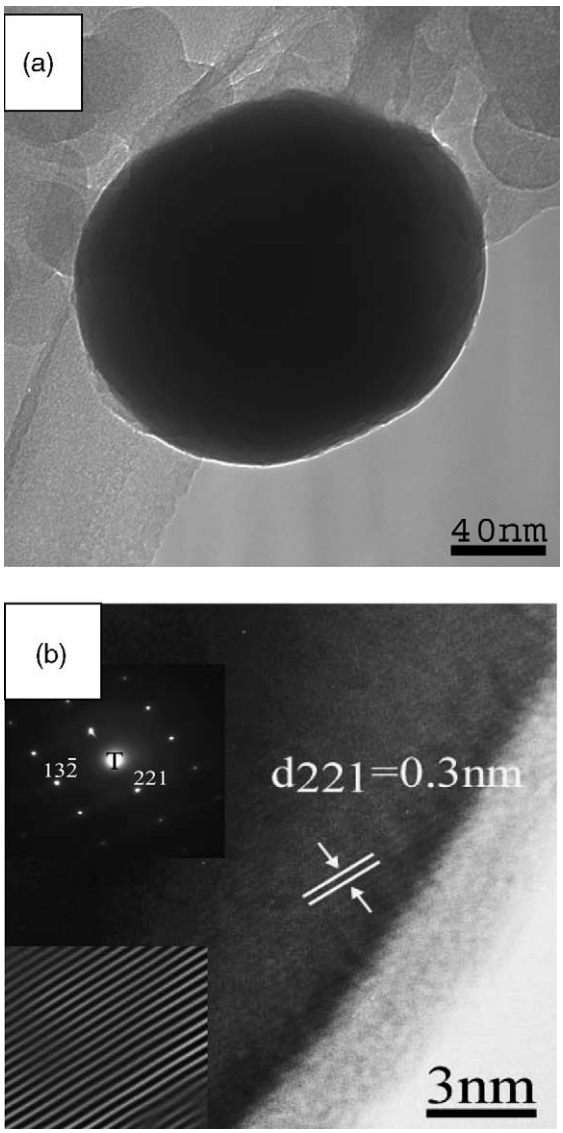


Fig. 6. Bright-field and high-resolution TEM image of lithiated Sn particle ($Li_7Sn_2$) discharged to 0.1 V at constant current density, 0.2 mA cm$^{-2}$.

and Fig. 5(b) shows a HRTEM image and [4 0 1] diffraction pattern of $Li_{13}Sn_5$ particles. The image of the atoms arranged in (0 1 0) planes can be seen clearly. The image of atoms in (0 1 0) corresponds to array of Sn atoms, whereas relatively light Li atoms are not seen. TEM photgraphas were also taken for Sn particles discharged to 0.1 V. The bright-field image, the HRTEM image and [7 5 4] diffraction pattern of $Li_7Sn_2$ particles are shown in Fig. 6. Lattice fringes of the (2 2 1) plane are seen in the HRTEM image (Fig. 6(b)).

The charge–discharge cycling performance of Sn powder electrodes with different average particle diameters is presented in Fig. 7. The nanometer-scale Sn powder electrode displays better cycling performance than the large particle Sn electrode. The former electrode has a more open structure and the binding agent (PVdF) is finely dispersed

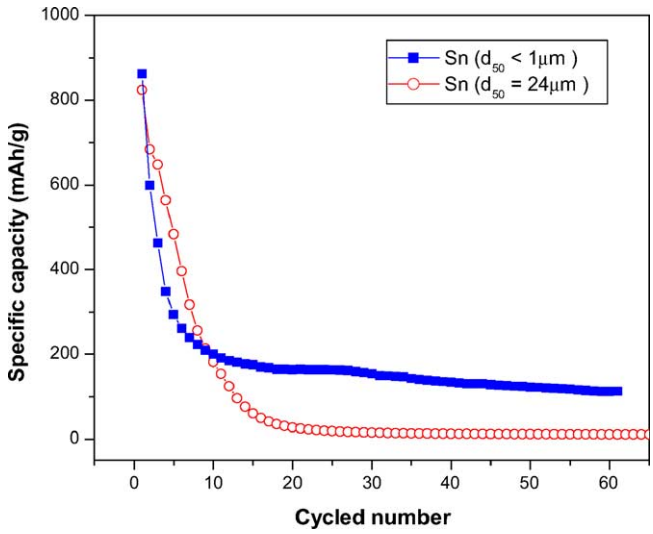


Fig. 7. Capacity vs. cycle number for nanometer-scale Sn/Li cell and lager particle Sn ($d_{50}$ = 24 μm)/Li cell measured at 0.2 mA cm$^{-2}$.

among the active materials (Sn particles), Such that the volume changes during Li insertion and de-insertion are more acceptable.

Fig. 8(a) shows FTIR spectra of a tin electrode discharged to 0.01 V and charged to 2.0 V at a constant current density of 0.02 mA cm$^{-2}$. There are many peaks due to the absorption of different chemical species. The peaks at 840 and 1276 cm$^{-1}$ ($PF_6^-$) correspond to the $LiPF_6$ in the electrolyte. The absorbance at the wave number, 1172 cm$^{-1}$ ($\nu_s$C=O) and 1488 cm$^{-1}$ ($\delta$C–H) shows the residual solvent, EC. The absorption bands at 1071 cm$^{-1}$ ($\nu$C–O), 1332 cm$^{-1}$ ($\nu_s$(C=O)), 1403 cm$^{-1}$ ($\delta$C–H), 1665 cm$^{-1}$ ($\nu_{as}$(C=O)) and 2942 cm$^{-1}$ ($\nu$C–H) are well in agreement with the IR spectrum for $ROCO_2Li$. The absorption band at 863 cm$^{-1}$ ($\delta CO_3^{2-}$) for the stable component, $Li_2CO_3$, is also present. These results indicate that the electrolyte and the solvent are decomposed into $ROCO_2Li$ and $Li_2CO_3$ on the surface of the tin powder during the stage of Li insertion. Aurbach et al. [17] have reported that the major surface species on graphite electrodes are $ROCO_2Li$ and $Li_2CO_3$. The former was formed by decomposition of solvent and the latter could be formed either by further reduction of $ROCO_2Li$ in the presence of Li ions, or by reaction of $ROCO_2Li$ with trace water [17]. Li et al. [19] showed that $Li_2CO_3$ and $C_2H_5OCO_2Li$ were formed on the surface of a nanometer-scale SnO electrode in 1 M $LiPF_6$/EC-DEC. The formation of a solid electrolyte interface (SEI) (or passivation layer) on a nanometer-scale tin powder electrode can be described by a similar mechanism to that a graphite electrode. When the tin powder is inserted with Li ions, the electrolyte decomposes to $ROCO_2Li$ on the surface of the tin electrode. With further discharge and charge, $Li_2CO_3$ is formed by reduction of $ROCO_2Li$ and the reaction of $ROCO_2Li$ with trace water. Fig. 8(b) shows an HRTEM image of SEI layer on the surface of a Sn electrode. The

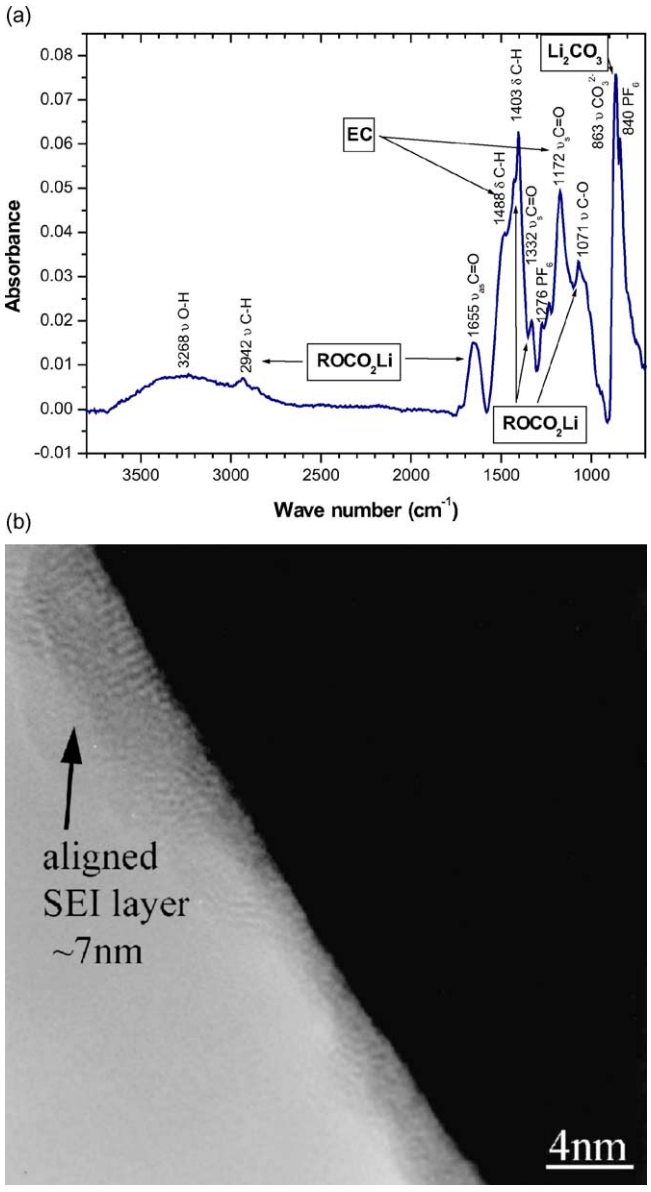


Fig. 8. (a) FT-IR spectra measured from nanometer-scale Sn electrode that was Li inserted and de-inserted in 1.3 M $LiPF_6$/EC-DEC (3:7) electrolyte and (b) high-resolution TEM image of SEI layer on surface of nanometer-scale Sn particle.

thickness of the SEI layer varies from 2 to 7 nm. In general the SEI layer appears to be in a non-crystalline state, but a poorly aligned structure is observed in the thick layer region. Dolle et al. [20] observed a SEI layer on the surface of carbon black powder discharged and charged with Li and using TEM, showed that its thickness was about 1.7 nm. Naji et al. [21] also found that the SEI layer on the surface of graphite anodes before and after discharge–charge in $LiClO_4$/EC consisted of polycrystalline $ROCO_2Li$ and $Li_2CO_3$ [21]. In our results, the SEI layer on the surface of the tin powder electrode is inhomogeneous in terms of microstructure and its thickness is larger than the layer formed on carbon black particles.

## 4. Conclusions

A nanometer-scale tin metal powder has been synthesized by the WEE method. From charge–discharge experiments and TEM observations it is proposed that Li–Sn alloys are formed during Li insertion into the tin metal. Stable Li–Sn alloys, such as $Li_{13}Sn_5$ and $Li_7Sn_2$, are formed together with meta-stable $Li_{1-x}Sn$. $Li_{1-x}Sn$ is considered to be an intermediate structure between tetragonal Sn and monoclinic LiSn during Li insertion into the tin metal. The main components of the SEI on the surface of the Sn electrode are $Li_2CO_3$ and $ROCO_2Li$ and the thickness of the SEI layer is 2–7 nm.

## Acknowledgements

The author would like to acknowledge support from the Ministry of Science & Technology of Korea through the National Research Laboratory Program.

## References

[1] K. Kinoshita, in: T. Osaka, M. Datta (Eds.), Energy Storage Systems for Electronics, Gordon and Breach Science Publishers, Singapore, 2000, p. 193.
[2] M. Winter, J.O. Besenhard, in: M. Wakihara, O. Yamamoto (Eds.), Lithium Ion Batteries: Fundamentals and Performance, Wiley–VCH, Weinheim, 1998, p. 173.
[3] I. Rom, M. Wachtler, I. Papst, M. Schmied, J.O. Besenhard, F. Hofer, M. Winter, Solid State Ionics 143 (1999) 329.
[4] M.M. Thackeray, J.T. Vaughey, C.S. Johnson, A.J. Kropf, R. Benedek, L.M.L. Fransson, Edstrom, J. Power Sources 113 (2003) 124.
[5] D. Fauteux, R. Koksbang, J. Appl. Electrochem. 23 (1993) 1.
[6] A.N. Dey, J. Electrochem. Soc. 118 (1971) 1545.
[7] N.P. Yao, L.A. Heredy, R.C. Saunders, J. Electrochem. Soc. 18 (1971) 1039.
[8] R.A. Sharma, R.N. Seefurth, J. Electrochem. Soc. 123 (1976) 1763.
[9] W. Weppner, R.A. Huggins, J. Electrochem. Soc. 25 (1978) 7.
[10] C.J. Wen, R.A. Huggins, J. Electrochem. Soc. 128 (1981) 1181.
[11] J. Wang, I.D. Raistrick, R.A. Huggins, J. Electrochem. Soc. 33 (1986) 457.
[12] R.A. Huggins, Solid State Ionics 113–115 (1998) 57.
[13] I.A. Courtney, J.R. Dahn, J. Electrochem. Soc. 144 (1997) 2045.
[14] J. Yang, M. Wachtler, M. Winter, J.O. Besenhard, Electrochem. Solid-State Lett. 2 (1999) 161.
[15] H. Li, X. Huang, L. Chen, Electrochem. Solid-State Lett. 1 (1998) 241.
[16] Y.S. Kwon, Y.H. Jung, N.A. Yavorovsky, A.P. Illyn, J.S. Kim, Scripta Mater. 44 (2001) 2247.
[17] D. Aurbach, B. Markovsky, I. Weissman, E. Levi, Y. Ein-Eli, Electrochim. Acta 45 (1999) 67.
[18] J.L.C. Daams, P. Villars, J.H.N. Vucht, Atlas of Crystal Structure Types for Intermetallic Phases, vol. 1, ASM International, p. 201.
[19] J. Li, H. Li, Z. Wang, L. Chen, X. Huang, J. Power Sources 107 (2002) 1.
[20] M. Dolle, S. Grugeon, L. Dupont, J-M. Tarascon, J. Power Sources 97-98 (2001) 104.
[21] A. Naji, J. Ghanbaja, B. Humbert, P. Willmann, D. Billaud, J. Power Sources 63 (1996) 33.